

**Quantum artificial intelligence for pattern recognition
at high-energy colliders:
Tales of Three “Quantum’s”**

Hideki Okawa

*Institute of High Energy Physics, Chinese Academy of Sciences,
Shijingshan, Beijing 100049, China*

okawa@ihep.ac.cn

Quantum computing applications are an emerging field in high-energy physics. Its ambitious fusion with artificial intelligence is expected to deliver significant efficiency gains over existing methods and/or enable computation from a fundamentally different perspective. High-energy physics is a big data science that utilizes large-scale facilities, detectors, high-performance computing, and its worldwide networks. The experimental workflow consumes a significant amount of computing resources, and its annual cost will continue to grow exponentially at future colliders. In particular, pattern recognition is one of the most crucial and computationally intensive tasks. Three types of quantum computing technologies, i.e., quantum gates, quantum annealing, and quantum-inspired, are all actively investigated for high-energy physics applications, and each has its pros and cons. This article reviews the current status of quantum computing applications for pattern recognition at high-energy colliders.

Keywords: high-energy colliders, quantum computing, quantum machine learning, pattern recognition, optimization

1. Introduction

The year 2025 marks the International Year of Quantum Science and Technology,¹ celebrating the 100th anniversary of the initial development of quantum mechanics, in particular, Heisenberg’s article “Quantum-mechanical re-interpretation of kinematic and mechanical relations”^{2a}. This work was established as matrix mechanics soon after, in collaboration with Born and Jordan.³ Schrödinger expanded the matter-wave concept introduced by De Broglie⁴ and formulated quantum mechanics as wave mechanics.⁵ Dirac⁶ and Jordan⁷ independently proved that these two formulations are equivalent. It may not be a mere coincidence that the notion of spin was proposed in the same year, 1925, by Uhlenbeck and Goudsmit.⁸

The first quantum revolution flourished in the 20th century through those paradigm shifts, enabling technologies such as lasers, transistors, magnetic resonance imaging, and semiconductors. We are now in the midst of the second quantum revolution, in which, for the first time in human history, we can identify and control

^aThis English translation of the original German title is taken from “Sources of Quantum Mechanics”, edited by B. L. van der Waerden (1967)

2 *Hideki Okawa*

a single quantum bit. It led to the arrival of commercial quantum computers, and quantum supremacy was demonstrated by Google Sycamore⁹ and Jiuzhang¹⁰ of the University of Science and Technology of China (USTC) in generating random states. However, we are still in the era of the so-called Noisy Intermediate-Scale Quantum (NISQ) computers,¹¹ and practical quantum advantage has yet to be established. Various distinctive technologies are being adopted for quantum computing hardware, and each has its pros and cons. A recent breakthrough by Google's Willow chip¹² has changed the landscape towards error correction. However, its impact on future pathways to large-scale, error-tolerant quantum computers and their practical applications remains to be seen. The Zuchongzhi 3.0 quantum computer by USTC has achieved performance comparable to Willow.¹³

An urgent need and interest in applying quantum computing and algorithms to high-energy physics (HEP) arise from the fact that future colliders will face an enormous increase in datasets in the coming decades. For example, at the High Luminosity Large Hadron Collider (HL-LHC),¹⁴ the computing time increases exponentially with pileup (additional proton-proton interactions per bunch crossing). It will reach exabyte-level data handling from the current petabyte level, leading to an annual cost increase by a factor of about 10 to 20.^{15,16} The Z -pole operation at the Circular Electron Positron Collider (CEPC)^{17,18} proposed in China will face similar computational challenges. Quantum computing and algorithms may allow us to overcome some of those challenges.

Applications of quantum computing to HEP can be categorized into two classes: (1) quantum machine learning and (2) quantum simulation^b. For the former, quantum properties such as the rich Hilbert space, superposition, entanglement (and tunneling for quantum annealing) could lead to improvement in learning data. For the latter, quantum computers simulate the time evolution of a given Hamiltonian; i.e., we can directly simulate quantum phenomena with quantum systems.

This article presents an overview of the brief history of quantum computing, the current state of quantum computing technologies (both described in Section 2), and its applications to experimental HEP, in particular for pattern recognition. As pattern recognition in HEP often amounts to optimization problems, Section 3 describes the formulation of Ising and quadratic unconstrained binary optimization (QUBO) problems and how quantum algorithms can solve them. Then, the current status of quantum artificial intelligence applied to track reconstruction and jet clustering is summarized in Sections 4 and 5, respectively. Reviews covering wider ranges of applications in experimental and theoretical HEP can be found in Refs. 19, 20, 21, 22, 23, 24, 25.

^bBe warned not to confuse with the simulation of quantum circuits by classical hardware. In this review, we will explicitly mention this case as a quantum circuit simulator.

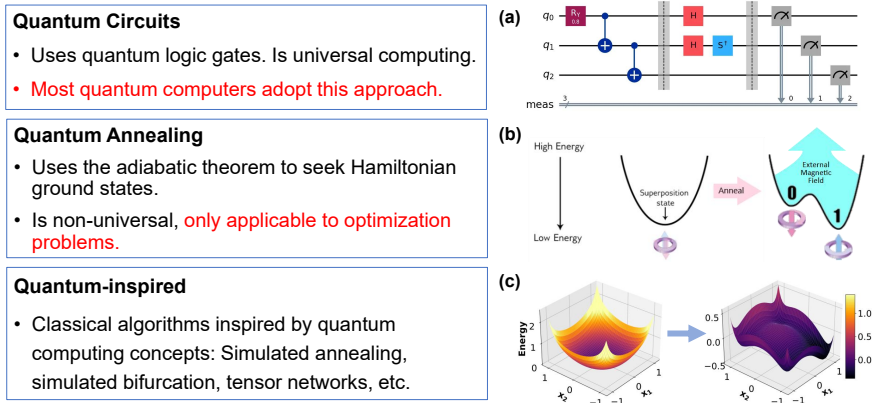


Fig. 1: Three types of quantum computing technologies: (a) quantum circuits, (b) quantum annealing (From Ref. 37, CC BY-NC-SA 4.0), and (c) quantum-inspired (courtesy: Xianzhe Tao).

2. Quantum Computing

The concept of quantum computing emerged in the early 1980s from several physicists.²⁶ In 1980, Manin proposed a quantum automaton based on superposition and entanglement,²⁷ and Benioff put forward a microscopic quantum-mechanical Hamiltonian as a model of Turing machines.²⁸ In 1981, Feynman delivered a presentation on the possibility of simulating quantum-mechanical effects in quantum systems,²⁹ which is the conceptual emergence of quantum simulation. Later on, Deutsch described a quantum Turing machine³⁰ for the first time, paving the way for universal quantum computation. Development of innovative quantum algorithms has followed, such as Shor’s factorization algorithm,³¹ which can crack the Rivest-Shamir-Adleman (RSA) encryption in polynomial time. Nakamura, Pashkin, and Tsai succeeded in realizing quantum bits in a superconducting material³² for the first time. Kadowaki and Nishimori proposed quantum annealing³³ in 1998, which led to the arrival of D-Wave’s commercial quantum annealers in 2011. IBM introduced the first circuit-based commercial computers in 2019.

Quantum computing can be categorized into three major classes using distinctive techniques (Fig. 1): quantum circuits (gate-based), quantum annealing, and quantum-inspired. The former two use quantum hardware, whereas the last uses “classical” hardware but algorithms inspired by quantum-computational ideas. There is another class of models called analog quantum computing, which often involves continuous variables.³⁴ However, its applications in HEP^{35,36} are currently limited and have not been considered for pattern recognition.

2.1. *Quantum circuits*

Quantum circuit hardware uses quantum logic gates, which perform unitary transformations. It was first defined in Ref. 38 and has been generalized in Ref. 39. It exploits universal computing, and thus most quantum computers adopt this approach. Quantum gates can be realized using various technologies, including superconductors, ion traps, photons, neutral atoms, silicon chips, and diamond. The superconducting technique is the most mature and scalable so far. Every approach has different performance and pros and cons in terms of the coherence longevity, processing speed, two-gate fidelity (i.e., logic success rate), connectivity, etc.

2.2. *Quantum annealing*

Quantum annealing uses the adiabatic theorem to seek the ground state of a given Hamiltonian.³³ It is non-universal computing and is only applicable to optimization problems described in Section 3. It is realized with a superconducting technique. Because of the fundamentally different implementation of the quantum circuits, quantum annealers already employ thousands of qubits. In addition to the quantum properties used in quantum circuits, quantum tunneling helps avoid the ground state prediction from being trapped in local minima. Section 3.1 describes the explicit formulation of how quantum annealing predicts the minimum energy of a Hamiltonian.

2.3. *Quantum-inspired*

An important class of quantum-inspired approaches solves optimization problems via “classical” time evolutions of differential equations. Because of its resemblance to the quantum-annealing approach, it is also called quantum-annealing-inspired algorithms (QAIA).⁴⁰ Simulated annealing (SA),⁴¹ simulated coherent Ising machines,⁴² and simulated bifurcation (SB)^{43–45} belong to this category. SA and SB have been considered in HEP applications; further details are provided in Section 3.3.

Another class of quantum-inspired algorithms actively investigated in high-energy physics is tensor networks (TNs). They have been used to represent quantum many-body systems on classical computers, which have naturally become a key component for simulating quantum circuits on classical hardware. They have also been actively used in theoretical HEP studies for particle dynamics. Their HEP applications to classification can be found in Refs. 46, 47, 48. As QAIA generally outperform TNs for optimization problems,⁴⁰ TNs have not been considered for pattern recognition in HEP and will not be covered in this review.

3. Ising/QUBO Problems

There is an important class of problems, the so-called combinatorial optimization problems. Practically complicated problems in society, such as route search, optimal

distribution and placement, and scheduling, can be formulated as such problems. They can be mapped to Ising or QUBO problems.⁴⁹ The difference between the two lies in using the ± 1 spins for the former or zero/one binaries for the latter. The Ising/QUBO problems are non-deterministic polynomial time (NP) complete; i.e., no efficient algorithm exists to find the solution. However, Ising problem solvers can provide quasi-optimal answers in a reasonable amount of time. Quantum computers and algorithms could also play crucial roles in addressing these challenges.

Solving the Ising problem is to find a spin configuration $\{x_i\}_{i=1}^N \in \{-1, 1\}^N$ that minimizes the Hamiltonian $H(x_i)$ of an Ising model with N spins:

$$H(x_i) = \frac{1}{2} \sum_{ij} J_{ij} x_i x_j + \sum_i h_i x_i, \quad (1)$$

where J_{ij} represents the spin-spin interactions and h_i is the external field. Similarly, a QUBO Hamiltonian can be formulated as:

$$O_{\text{QUBO}}(s_i) = \sum_{i,j=1}^N Q_{ij} s_i s_j, \quad (2)$$

where s_i is the binary $\{0,1\}$ and Q_{ij} is the QUBO matrix. The QUBO and Ising Hamiltonians can be converted to each other by:

$$x_i \longleftrightarrow 2s_i - 1, \quad (3)$$

$$J_{ij} \longleftrightarrow \frac{Q_{ij}}{2}, \quad (4)$$

$$h_i \longleftrightarrow \frac{\sum_j Q_{ij}}{2}. \quad (5)$$

Various components of workflow in high-energy collider experiments can also be regarded as optimization procedures. Below are outlined algorithms for addressing optimization problems using the three quantum technologies.

3.1. Solving Ising problems with quantum annealing

Quantum annealing simulates the time evolution of the Transverse Field Ising Model relying on the adiabatic theorem (Fig. 1 (b)), with the Hamiltonian H given by:

$$H(s) = A(s)H_{\text{initial}} + B(s)H_{\text{target}}, \quad (6)$$

where s is the normalized time parameter, and H_{initial} is the initial Hamiltonian of the system, taken to be a transverse field, typically defined as:

$$H_{\text{initial}} = \sum_i \sigma_i^x. \quad (7)$$

σ_i^x is the Pauli X matrix operating on the i -th qubit. H_{target} is the unknown ground state of the Ising Hamiltonian, representing the target optimization function:

$$H_{\text{target}} = \sum_{ij} J_{ij} \sigma_i^z \sigma_j^z + \sum_i h_i \sigma_i^z, \quad (8)$$

6 *Hideki Okawa*

where J_{ij} is the coupling strength between the i -th and j -th qubits, σ_i^z is the Pauli Z matrix operating on the i -th qubit, and h_i is the strength of the external longitudinal field applied to the i -th qubit. $A(s)$ and $B(s)$ are the annealing schedules of the Hamiltonian. Measuring the final state would provide the solution to the Ising problem.

3.2. Solving Ising problems with quantum circuits

Quantum circuit machines can also solve Ising problems using variational circuits. Quantum-classical hybrid methods such as Variational Quantum Eigensolver (VQE)⁵⁰ and Quantum Approximate Optimization Algorithm (QAOA)^{51,52} fall into this category. The principle of QAOA is described below as an example.

QAOA mimics the quantum annealing procedure by performing Trotterization of the Hamiltonian and searching for the ground state by scanning the variational parameters with classical optimizers. It consists of a quantum component that prepares a quantum state using a set of variational parameters, and a classical component that fine-tunes those parameters and returns them to the quantum component in a continuous feedback loop. The adiabatic evolution is defined the same as in Eq. 6, with the linear annealing schedule ($A(s) = 1 - s$ and $B(s) = s$) usually adopted in QAOA. For each distinct parameter p , which corresponds to the circuit depth, sets of variational initial values for various QAOA circuit parameters are randomly generated. The Trotterization operation U is pursued in sufficiently small time steps Δt :

$$\begin{aligned} U &\approx \prod_{n=1}^p e^{-iH(n\Delta t)\Delta t} = \prod_{n=1}^p e^{-i(1-s(n\Delta t))H_{\text{initial}}\Delta t} e^{-is(n\Delta t)H_{\text{target}}\Delta t} \\ &= \prod_{n=1}^p e^{-i\beta_n H_{\text{initial}}} e^{-i\gamma_n H_{\text{target}}} = \prod_{n=1}^p U_M(\beta_n) U_C(\gamma_n), \end{aligned} \quad (9)$$

where β_n and γ_n are variational parameters, $U_C(\gamma_n)$ ($U_M(\beta_n)$) is the operation of consecutive cost (mixer) layers in QAOA. Executing the quantum circuits with the optimized variational parameters yields a specific quantum state that should correspond to the answer to the Ising problem. However, QAOA suffers from adiabatic bottlenecks and requires a large circuit. Scaling QAOA to large problems encounters Barren plateaus and is known to be challenging. A recent development of an imaginary Hamiltonian variational Ansatz (iHVA)⁵³ and Imaginary Time Evolution-Mimicking Circuit (ITEMC)⁵⁴ overcomes those bottlenecks of QAOA, and they are validated up to a graph with 67 (80) nodes for the former (latter).

3.3. Solving Ising problems with quantum-inspired algorithms

SA has been actively considered for optimization problems in HEP, recently as a benchmark to evaluate the effectiveness of quantum annealing, but also as a stand-alone option with dedicated hardware, such as digital annealing.⁵⁵ Applications

of SB in HEP have recently emerged as a promising option^{56,57} due to its strong affinity with multiple processing and cutting-edge computing resources, such as graphical processing units (GPUs) and field-programmable gate arrays (FPGAs). The mechanisms of these quantum-inspired algorithms are briefly described below.

3.3.1. Simulated annealing (SA)

SA employs random movements throughout the solution space to search for the global minimum.⁴¹ Analogous to the process of determining the ground state of matter, a “temperature” is introduced to initially “melt” a substance at a high temperature, and then, the temperature is gradually decreased until the system “freezes”, resembling the formation of a crystal from a molten state. A simple algorithm proposed in Ref. 58 is used for the iteration, which applies a small random displacement to the original spin configuration and computes the energy difference ΔE . If $\Delta E < 0$, then the new configuration is immediately accepted as the temporary prediction, and the algorithm proceeds to the next iteration. Conversely, if $\Delta E > 0$, the new configuration is accepted only probabilistically, according to the Boltzmann factor $P(\Delta E) = \exp(-\Delta E/k_B T)$, which is introduced to avoid local minima. The process continues until the energy stabilizes or is terminated by a user-defined duration.

3.3.2. Simulated bifurcation (SB)

SB addresses combinatorial optimization problems via the adiabatic evolution of Kerr-nonlinear parametric oscillators (KPOs), which exhibit bifurcations corresponding to the two Ising spin states. The real and imaginary parts of the KPO amplitudes are interpreted as the positions x_i and momenta y_i of virtual particles. Taking the sign of the particle positions, $\text{sgn}(x_i)$, determines the spin. SB can update all oscillators in parallel, thereby accelerating computation. This feature is in clear contrast to SA, which generally cannot update spins independently. However, the original version of SB, adiabatic SB (aSB),⁴³ is prone to errors originating from the continuous treatment of the spins x_i in the differential equations. To mitigate these analog errors, two variants of SB are introduced: ballistic SB (bSB) and discrete SB (dSB).⁴⁴ Inelastic walls are introduced at $x_i = \pm 1$ for both, and x_j is discretized to $\text{sgn}(x_j)$ in the mean-field term for dSB to suppress the error from the

8 *Hideki Okawa*continuous relaxation of x_i :

$$\dot{x}_i = \frac{\partial H_{\text{SB}}}{\partial y_i} = a_0 y_i, \quad (10)$$

$$\begin{aligned} \dot{y}_i &= -\frac{\partial H_{\text{SB}}}{\partial x_i}, \\ &= \begin{cases} -[a_0 - a(t)]x_i + c_0 \left(h_i + \sum_{j=1}^N J_{ij} x_j \right), [\text{bSB}] \\ -[a_0 - a(t)]x_i + c_0 \left(\sum_{j=1}^N J_{ij} \text{sgn}(x_j) + h_i \right), [\text{dSB}] \end{cases} \end{aligned} \quad (11)$$

$$(12)$$

where a_0 is the positive detuning frequency, c_0 represents the positive coupling strength, and $a(t)$ denotes a time-dependent pumping amplitude that monotonically increases from zero to a_0 . J_{ij} and h_i are the spin-spin interactions and the external field, respectively, given by the Ising problem (Eq. 1) under consideration. The Hamiltonian of the non-linear oscillator system H_{SB} and its potential energy V_{SB} are defined as:

$$H_{\text{SB}} = \frac{a_0}{2} \sum_{i=1}^N y_i^2 + V_{\text{SB}}, \quad (13)$$

$$V_{\text{SB}} = \begin{cases} \frac{a_0 - a(t)}{2} \sum_{i=1}^N x_i^2 - c_0 \left(\frac{1}{2} \sum_{i,j} J_{ij} x_i x_j + \sum_i h_i x_i \right), [\text{bSB}] \\ \frac{a_0 - a(t)}{2} \sum_{i=1}^N x_i^2 - c_0 \left(\frac{1}{2} \sum_{i,j} J_{ij} x_i \text{sgn}(x_j) + \sum_j h_j x_i \right), [\text{dSB}] \\ \forall x_i, |x_i| \leq 1 \\ \infty, \text{ otherwise } [\text{bSB}, \text{dSB}] \end{cases} \quad (14)$$

Finally, as stated above, $\text{sgn}(x_i)$ gives the solution to the Ising problem. For all SB variants, numerical computations are performed using the symplectic Euler method.⁵⁹ Another set of variants that introduces heat fluctuations⁴⁵ has a relatively mild impact on the performance and is currently not considered in HEP.

4. Track reconstruction

Track reconstruction or tracking is a pattern recognition procedure to recover trajectories of charged particles and measure their momenta from hits in the silicon detector layers and/or drift chambers (Fig. 2). Track reconstruction algorithms determine how to assign the detector hits to form track candidates, i.e. so-called track finding, and then pursue track fitting to obtain helix parameters. The combined Kalman filter is actively used in various experiments for track finding and is adopted in A Common Tracking Software (ACTS),⁶⁰ for example. Recently, machine learning approaches such as Graph Neural Networks (GNNs)^{61–63} and Transformers^{64–67} are also gaining attention for track finding. The least squares (χ^2) or Runge-Kutta method is frequently used for track fitting. Those tracks are then used to reconstruct vertices and physics analysis objects further.

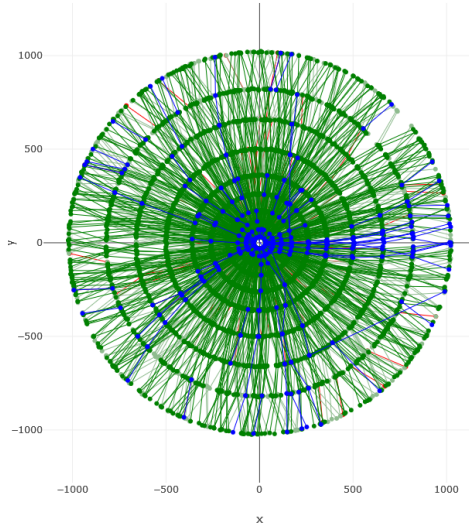


Fig. 2: Display of reconstructed tracks in an event from the TrackML dataset,^{68,69} which is simulated under the HL-LHC conditions. The green (red) lines represent tracks that are correctly (incorrectly) reconstructed, whereas the blue lines are unreconstructed tracks. Reproduced from Ref. 56. CC BY 4.0.

Applications of quantum algorithms can be categorized into two classes of reconstruction: (1) a global method that formulates track finding as an Ising/QUBO problem and (2) an iterative method that attempts to replace existing classical computation by quantum algorithms.

4.1. Global track finding as an Ising problem

Formulating track finding as an optimization problem dates back to the Denby-Peterson method,^{70,71} which used neural networks or cellular automata to predict the ground state of a proposed Hamiltonian resembling a QUBO. The method was later employed at the ALEPH,⁷² ARES,⁷³ ALICE,⁷⁴ and LHCb⁷⁵ experiments. In those studies, all potential combinations of two detector hits, i.e., doublets, were generated and subjected to some quality criteria. The algorithm performed binary classification to determine which doublet combinations should be retained to form track candidates. Two pioneering works applying quantum algorithms used quantum annealing^{76,77} with either doublets or triplets (i.e., segments of three detector hits) to reconstruct tracks.

Ref. 76 adopted a doublet-based approach and modified the Denby-Peterson

Table 1: Parameters that enter the definition of the modified Denby-Peterson QUBO (Eq. 15).⁷⁶ The description corresponds to what the parameters are designed for.

Parameter	Value	Description
λ	13.17	Track angle separator
ρ	5.00	High-momentum bias
η	14.41	Beam spot bias
ζ	1.79	Beam spot separator
α	86.20	Bifurcation penalty
β	20.91	Edge alignment penalty
γ	9.79	Total edge count penalty

Hamiltonian^{70,71} to match the HL-LHC configuration as:

$$\begin{aligned}
E = & - \sum_{a,b,c} \left(\frac{\cos^\lambda(\theta_{abc}) + \rho \cos^\lambda(\phi_{abc})}{r_{ab} + r_{bc}} \right) s_{ab}s_{bc} + \eta \sum_{a,b,c} \left(z_c - \frac{z_c - z_a}{r_c - r_a} r_c \right)^\zeta s_{ab}s_{bc} \\
& + \alpha \left(\sum_{b \neq c} s_{ab}s_{ac} + \sum_{a \neq c} s_{ab}s_{cb} \right) - \sum_{a,b} (\beta P(s_{ab}) - \gamma) s_{ab},
\end{aligned} \tag{15}$$

where E is the QUBO Hamiltonian; a, b, c are the detector-hit labels for the two connected doublets; θ_{abc} (ϕ_{abc}) is the Cartesian (azimuthal) angle between the doublets; r_{ab}, r_{bc} are the doublet lengths; s_{ab}, s_{bc} are the binary variables to define whether those doublets should be kept; z, r are the hit location in the rz -plane^c; $P(s_{ab})$ is the prior probability for the given doublet using a Gaussian kernel density estimation (KDE); and $\lambda, \rho, \eta, \zeta, \alpha, \beta, \gamma$ are parameters defined in Table 1, determined by Bayesian optimization. The parameters are chosen to provide the best performance with SA in terms of the harmonic mean of track reconstruction efficiency and purity, defined as:

$$\text{Efficiency (Recall)} = \frac{\text{The number of correctly reconstructed doublets}}{\text{The number of true doublets}}, \tag{16}$$

$$\text{Purity (Precision)} = \frac{\text{The number of correctly reconstructed doublets}}{\text{The number of all reconstructed doublets}}. \tag{17}$$

The track reconstruction performance was evaluated using the TrackML Challenge dataset.^{68,69} This dataset simulates a top-quark pair process generated with Pythia8⁷⁸ with additional 200 proton-proton interactions overlaid that align with the HL-LHC conditions, along with a fast detector simulation. The D-Wave 2X quantum annealer with 1,098 qubits and SA demonstrated promising and comparable track reconstruction efficiency and purity up to 500 particles. Track finding

^cThe z -axis is chosen to align with the beam direction at the collider experiments, and r is the distance in polar coordinates in the plane perpendicular to the beam axis.

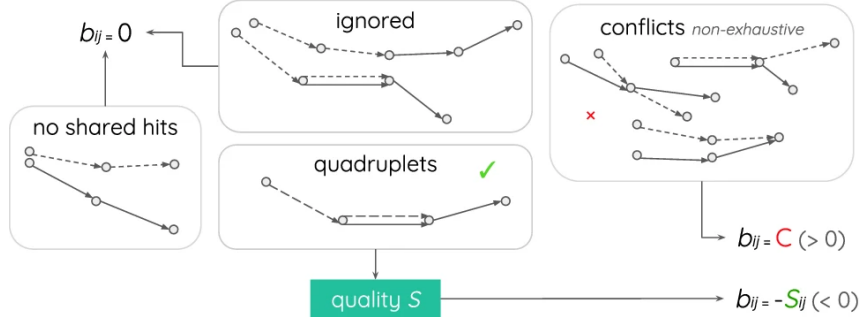


Fig. 3: Criteria for assigning QUBO quadratic coefficients depending on the configurations of triplet pairs. Reproduced from Ref. 77. CC BY 4.0.

for events with more particles could not be pursued due to the limited number of qubits and connectivity in D-Wave hardware. The SA results up to 1,000 particles showed that the track reconstruction performance does not degrade with higher multiplicity.

LHCb recently investigated a similar doublet-based method using a Denby-Peterson Hamiltonian.⁷⁹ They first evaluated the method with a classical solver on $B_s \rightarrow \phi\phi$ events using the full detector simulation and obtained a performance comparable to the state-of-the-art approach at the LHCb, i.e., Search-by-Triplet.⁸⁰ Then, they moved on to testing the quantum Harrow-Hassadim-Lloyd (HHL) algorithm⁸¹ for the Hamiltonian minimization for events up to five particle multiplicity with a simple detector toy model.⁸² A noiseless quantum circuit simulator, Qiskit Aer, pursued the HHL algorithm up to 14 qubits, and the quantum circuit was designed to fit the `ibm_hanoi` 27-qubit r5.11 Falcon quantum processor. Hit purity and efficiency of 100% can be achieved for the simple toy model events, but require a few thousand to tens of millions of circuit depth, which is unfeasible for current circuit-based quantum hardware.

The other pioneering quantum annealing approach adopted triplets instead.⁷⁷ The triplet-based QUBO Hamiltonian is defined as:

$$O(a, b, T) = \sum_{i=1}^N a_i T_i + \sum_{i=1}^N \sum_{j<i}^N b_{ij} T_i T_j, \quad (18)$$

where N is the number of triplets, T_i and T_j correspond to the binaries for the triplets, a_i is the bias weight used to evaluate the quality of the triplets, and b_{ij} is the coefficient that quantifies the compatibility of two triplets (Fig. 3: $b_{ij} = 0$ if they share no hit, $= 1$ if there is any conflict, and $= -S_{ij}$ if they share two hits). As the coefficients a_i and b_{ij} are unitless, the objective QUBO Hamiltonian $O(a, b, T)$ is accordingly unitless. The coefficient $-S_{ij}$ quantifies the consistency of the two triplet momenta via the curvature and the angle of the two triplets.⁷⁷ The bias weight a_i has a significant impact on the Hamiltonian energy landscape, track reconstruction purity, and computation speed. It is a function of the transverse and longitudinal

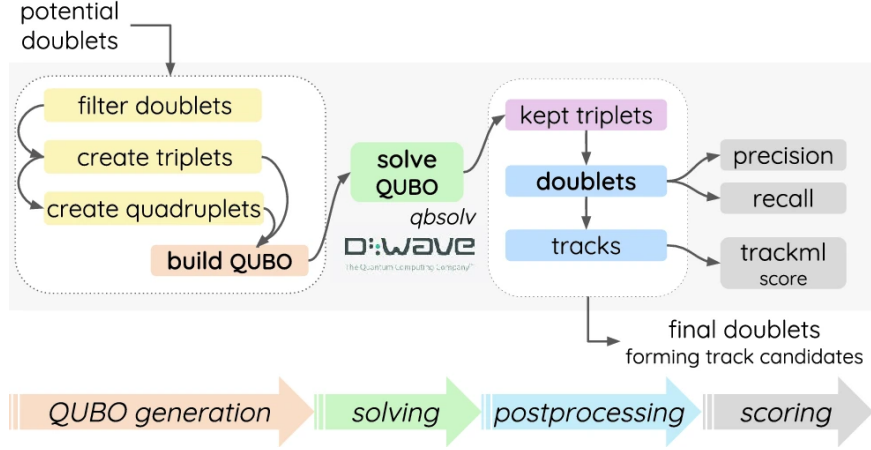


Fig. 4: Schematic overview of tracking workflow using the QUBO formulation (b). Reproduced from Ref. 77. CC BY 4.0.

displacements of the triplets from the primary vertex (the most significant proton-proton collision point of an event), optimized with tunable parameters.⁷⁷ The overall workflow of global track finding is schematically described in Fig. 4. The “solving” part could be pursued with any other Ising problem solvers, such as VQE, QAOA, or quantum-inspired algorithms. This study has also adopted the TrackML Challenge dataset and evaluated up to 6,600 tracks. D-Wave 2X hardware and D-Wave Neal SA provided comparable performance; efficiency remained relatively stable, whereas purity tends to degrade against the track multiplicity.

A notable difference in the approach between Refs. 76 and 77 is that the Ising problem was split into sub-matrices and the optimization is iteratively pursued for the latter, in order to handle the high track multiplicity events. This approach is called the sub-QUBO method (Fig. 5). The track multiplicity is exceedingly high at the HL-LHC, leading to about 0.1M spins/binaries or more in the Ising/QUBO formulation. Such large problems obviously do not fit in existing quantum circuits and annealing hardware. D-Wave provides the qbsolv sub-QUBO solver, which has been used in Refs. 77, 83, 84, 85, for example. Refs. 83, 84 performed track reconstruction on a simulated dataset from the LUXE experiment,⁸⁶ where qbsolv was used along with VQE. Its track reconstruction performance was comparable to the traditional combined Kalman filter. In Ref. 85, the dependence of the tracking performance on the sub-QUBO matrix sizes was evaluated. It is worth noting that most sub-QUBO approaches, including qbsolv, are heuristic and lack a theoretical foundation. Ref. 87 adopted, for the first time in HEP, a theoretically robust sub-QUBO algorithm using multiple solution instances.⁸⁸ The study also introduced QAOA for the first time in track finding,⁸⁷ and achieved comparable performance to the D-Wave results⁷⁷ using 6-qubit Origin Quantum Wuyuan hardware.

The tracking studies using quantum annealing or circuit hardware all obtained

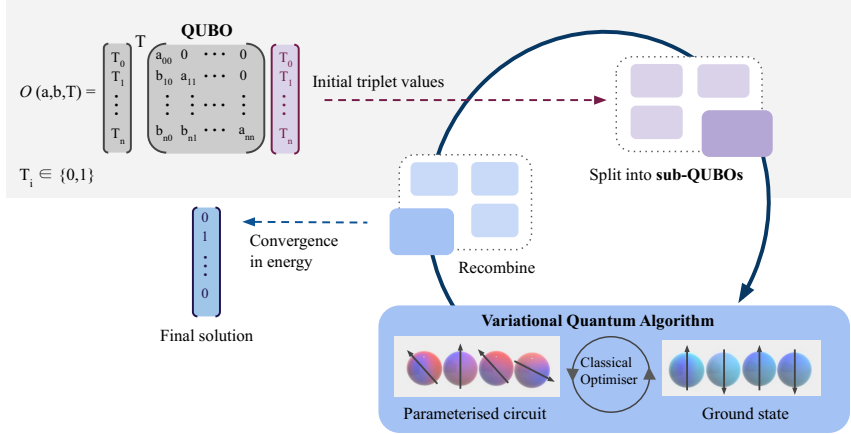


Fig. 5: Schematic diagram illustrating the sub-QUBO procedure. Reproduced from Ref. 84. CC BY 4.0.

performance comparable to the traditional methods. However, the critical bottleneck from the limited hardware resources remains. The sub-QUBO approach generally does not lead to degradation in the Ising solving precision itself, but the computational speed degrades by two orders of magnitude⁷⁷ or more, depending on the fineness of the sub-QUBO splitting. In order to overcome this challenge, Ref. 56 investigated quantum-inspired algorithms, bSB, dSB, and D-Wave Neal SA in particular, as they can directly handle the HL-LHC dataset. Figs. 6a and 6b show the track reconstruction performance in terms of efficiency and purity. The SB algorithms provide comparable or slightly better efficiency and purity than D-Wave Neal SA. Using a single GPU, bSB achieves four orders of magnitude speed-up from D-Wave Neal SA (Fig. 6c): the reduction from 23 minutes down to 0.14s, for the largest TrackML dataset of 9,435 particle multiplicity (Fig. 2 shows its event display). SB can effectively run multiple processing tasks with cutting-edge computing resources such as GPU and FPGA, demonstrating its potential and readiness for practical applications.

A distinctive approach is to regard track reconstruction as a classification of signal and background events from the detector hits,⁸⁹ formulated as an optimization problem. The classification can be pursued with the quantum associative memory model (QAMM)^{90,91} or the quantum content addressable memory model (QCAM)⁹² on the D-Wave 2000Q quantum annealer. The study considered two classification methods: the first based on the solution state energy and the second based on the key bit value for the classification label. The optimal choice of the memory and classification method depends on the track density. The performance is highly sensitive to the pattern density α and degrades for large densities.

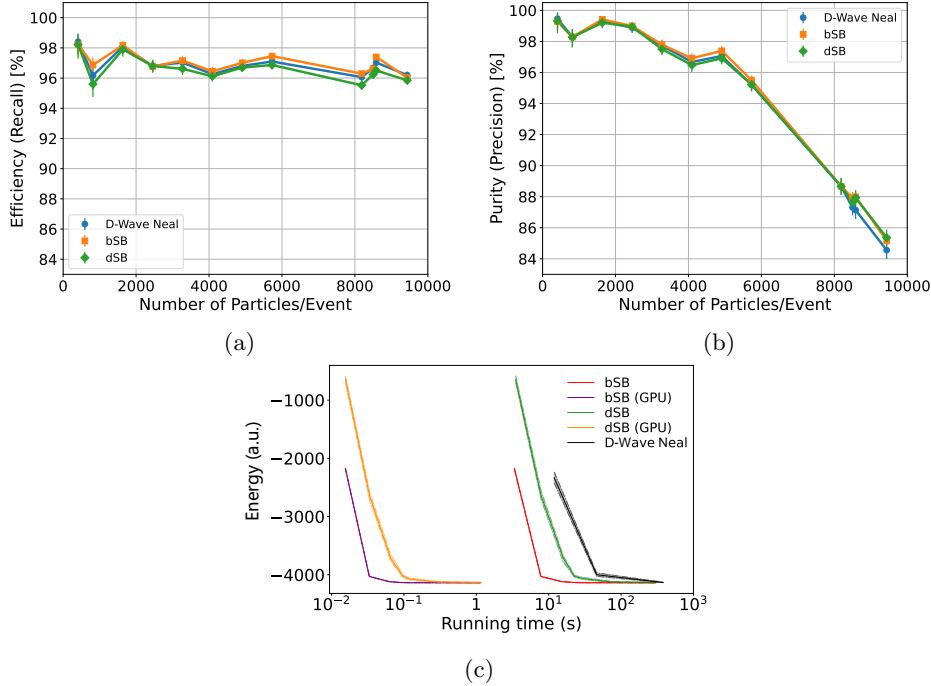


Fig. 6: Efficiency (recall) (a) and purity (precision) (b) in relation to particle multiplicity, and evolution of Ising energies over time for the event with the highest particle multiplicity (c) evaluated for the three quantum-inspired algorithms. Reproduced from Ref. 56. CC BY 4.0.

4.2. Global track finding with neural networks or kernels

As mentioned above, classical GNNs have been actively investigated at various collider experiments. In the GNN approach, detector hits are regarded as nodes and connected track segments as edges. The empirical evidence shows that the computing time scales linearly with the number of space points.⁶¹ This feature is in clear contrast to the exponential increase observed in the combined Kalman filter.

To explore potential benefits from variational quantum layers, a hybrid quantum-classical GNN (QGNN) was developed for track reconstruction.⁹³ The QGNN consists of three networks as schematically presented in Fig. 7. The Input Network accepts the spatial coordinates of the detector hits to a fully connected neural network layer to form the initial node feature vector. Then the node feature vector is passed to Edge and Node Networks that iteratively process the graph to determine the final edge probabilities. In those networks, both classical and quantum layers are combined to form Hybrid Neural Networks (HNNs) (Fig. 8). The information encoding circuit (IEC) maps classical data to qubits. The parameter-

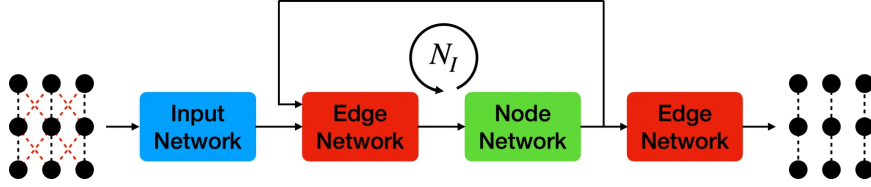


Fig. 7: Schematic presentation of the QGNN architecture. Reproduced from Ref. 93. CC BY 4.0.

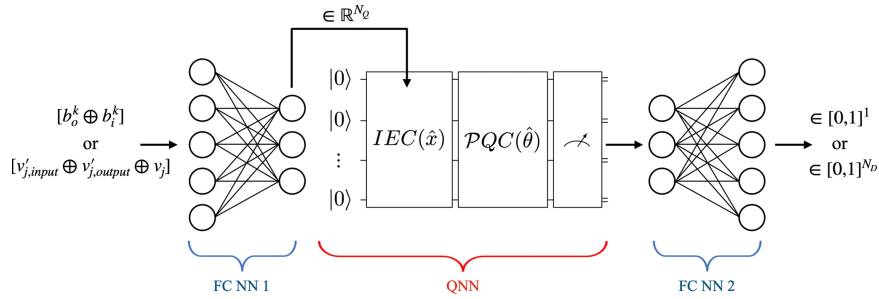


Fig. 8: The Hybrid Neural Network architecture consists of classical and quantum layers. Reproduced from Ref. 93. CC BY 4.0.

ized quantum circuit (PQC) transforms those states to the Hilbert space. Finally, measurements are passed back to the classical layers. Four different configurations of PQCs are investigated in the study, for two of which originate from tensor networks: matrix product state (MPS) and Tree Tensor Network (TTN).

The study showed that the expressibility and entanglement capacities of the quantum circuits affect the training performance. Because of quantum hardware limitations, the study was conducted with a quantum circuit simulator handling up to 16 qubits.^{93,94} The QGNN model achieves comparable performance to the classical counterpart. It adopted angle encoding, but more sophisticated encoding has the potential to improve the performance and is left for future studies. The algorithm was also adopted for a LUXE simulation dataset⁸⁴ via a quantum circuit simulator, achieving a comparable efficiency to the traditional combined Kalman filter and the VQE algorithm, but with a visibly higher fake rate. Evaluating the impact of hardware noise and performing the algorithm on quantum hardware is left for future studies. A QUBO version of GNN tracking was investigated in Ref. 95.

An alternative approach was proposed to classify triplets as being associated with the same track or not, based on a support vector machine (SVM) with a quantum-estimated kernel.⁹⁶ The quantum-kernel approach outperforms its classical counterpart for datasets with many features. However, specifically for triplet-based cases, the quantum-enhanced method did not bring in any benefit.

4.3. Iterative quantum tracking

Iterative track reconstruction requires Associative Memory to store a database that encompasses hit patterns in the detector. The software prototype of Quantum Associative Memory (QuAM)^{97–99} using a quantum circuit was discussed for data triggering at the LHC.¹⁰⁰ An exponential capacity increase with QuAM was conceptually demonstrated, but its practical implementations in IBM 5Q and 14Q quantum hardware faced some topological bottlenecks because of the limited number of qubits and their connectivity.

The whole reconstruction chain on a realistic dataset is presently unfeasible to pursue on quantum hardware; however, its computational complexity was evaluated for each step:¹⁰¹ seeding, track building, cleaning, and final selection. In contrast to the majority of the global reconstruction studies that concentrate on the track building step, this study outlines the complexity of algorithms at each tracking stage, as summarized in Table 2. The algorithm used at the CMS experiment¹⁰² was adopted as the classical benchmark. At the seeding stage, we form initial track segments with just a few detector hits. Seeding uses the Grover search algorithm^{103,104} for the quantum approach, leading to the quantum complexity of $\tilde{O}(\sqrt{k_{\text{seed}} \cdot n^c})$ instead of $O(n^c)$ from the classical algorithm, where k_{seed} is the number of seeds, n is the number of charged particles in the events, and c is the number of detector hits used for the seeds. Then, for track building, those seed trajectories are extrapolated along the expected path, adding compatible detector hits with the lowest χ^2 from the consecutive detector layers to form track candidates. The quantum minimum finding algorithm by Dürr and Høyer¹⁰⁵ allows us to find the best track candidates with $\tilde{O}(k_{\text{seed}} \cdot \sqrt{n})$ instead of the classical complexity of $\tilde{O}(k_{\text{seed}} \cdot n)$. As multiple track candidates could describe the same particle, a cleaning process removes track candidates that share the majority of the detector hits. Finally, only the track candidates satisfying some criteria based on the trajectory fit quality are kept as the final tracks. The study demonstrated that quantum algorithms can reconstruct the same tracks as the classical algorithm with lower quantum complexity, in particular for seeding and track building. However, the expected quantum advantage with this approach is rather mild, and the authors speculate on a potentially higher success in designing a completely new algorithm, which aligns with the directions already mentioned in Sections 4.1 and 4.2.

An alternative iterative approach using a novel oracle design was proposed in Ref. 106, which extends the idea of using QuAM.¹⁰⁰ The study considered a simplified detector model with four layers of three tracking modules and used a quantum circuit simulator to demonstrate the performance. Track reconstruction with a quantum version of the template matching algorithm^{107–110} was considered. The study adopted a generalization of the Grover search algorithm: Quantum Amplitude Amplification (QAA),¹¹¹ which improves the efficiency of database encoding. QAA consists of two components: the oracle, which labels the states of interest by inverting their phase, and the diffuser, which enlarges the amplitudes of the marked states

Table 2: Computational complexity of track reconstruction at each stage with classical and quantum algorithms.¹⁰¹ k_{cand} is the number of track candidates. The original version of the cleaning stage refers to the method used by the CMS experiment,¹⁰² whereas the authors of this study found an algorithm with lower complexity.¹⁰¹

Tracking stages	Input size	Output size	Classical complexity	Quantum complexity
Seeding	$O(n)$	k_{seed}	$O(n^c)$	$\tilde{O}(\sqrt{k_{\text{seed}} \cdot n^c})$
Track Building	$k_{\text{seed}} + O(n)$	k_{cand}	$O(k_{\text{seed}} \cdot n)$	$O(k_{\text{seed}} \cdot \sqrt{n})$
Cleaning (original)	k_{cand}	$O(k_{\text{cand}})$	$O(k_{\text{cand}}^2)$	–
Cleaning (improved)	k_{cand}	$O(k_{\text{cand}})$	$O(k_{\text{cand}})$	–
Selection	$O(k_{\text{cand}})$	$O(k_{\text{cand}})$	$O(k_{\text{cand}})$	–
Full Reconstruction	n	$O(n^c)$	$O(n^{c+1})$	$\tilde{O}(n^{c+0.5})$
Full Reconstruction with $O(n)$ reconstructed tracks	n	$O(n)$	$O(n^{c+1})$	$\tilde{O}(n^{(c+3)/2})$

(Fig. 9). To match the 12-module simplified detector, the study used 12 qubits to perform QAA. As the Quantum Random-Access Memory (QRAM)¹¹² is not available, the database is prepared via the state preparation routine in IBM Qiskit. It uses a recursive initialization algorithm with optimization.¹¹³ The quantum circuit consists of the data and template registers, following the oracle construction from Ref. 114. The detector hits are encoded onto the data register, and the template register encodes the QAA routine with the unitary operations \mathcal{A}_D and \mathcal{A}_T , respectively. For the simplified dataset under consideration, 15 possible patterns exist and are one-hot encoded into bit strings of 12 qubits, with each bit corresponding to the detector module. When a module detects a hit, its bit is flipped to “1”; otherwise, it remains as “0”. Then the general oracle marks the state in the template database that corresponds to the detector hit pattern encoded on the data register. The diffuser operators then amplify the marked amplitudes. With three iterations of the QAA routines and 10^4 shots on the qasm_simulator without a noise model, this method achieved a track finding efficiency larger than 90% for events without any detector failure. The study also demonstrated that the oracle can be modified to account for missing hits from detector failures. Notably, this modification does not lead to additional computational complexity, which is in clear contrast to classical techniques.

4.4. Vertex reconstruction

Primary vertices are positions of beam-particle interactions at high-energy colliders and are crucial components to fully reconstruct collision events based on the detector information. Primary vertices are reconstructed by clustering charged-particle tracks along the beam axis. Ref. 115 developed a quantum-annealing approach to reconstruct primary vertices from simplified artificial datasets, which resemble conditions in the Compact Muon Solenoid (CMS) experiment at the LHC.

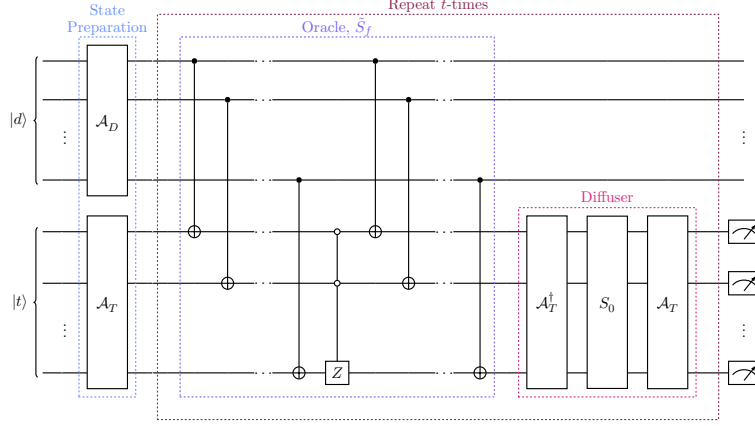


Fig. 9: Schematic circuit diagram of Quantum Amplitude Amplification (QAA). Reproduced from Ref. 106. CC BY 4.0.

To cluster the tracks, the QUBO Hamiltonian Q_{vtx} was defined as:

$$Q_{\text{vtx}} = \sum_k^{n_V} \sum_i^{n_T} \sum_{j>i}^{n_T} p_{ik} p_{jk} g(D(i, j); m) + \lambda \sum_i^{n_V} \left(1 - \sum_k^{n_V} p_{ik} \right), \quad (19)$$

where i and j are indices for tracks, k is the index for vertices, n_V is the number of vertices, n_T is the number of tracks, and p_{ik} is the probability of the i -th track to be associated with the k -th vertex. g is a distortion function that measures the deformation between a source and its measurement, m is a distortion parameter, and $D(i, j)$ is a distance metric between the i -th and j -th tracks. g and $D(i, j)$ are defined as:

$$g(x, m) = 1 - e^{-mx}, \quad (20)$$

$$D(i, j) = \frac{|z_i - z_j|}{\sqrt{\delta z_i^2 + \delta z_j^2}}, \quad (21)$$

where z_i is the longitudinal displacement parameter z_0 of the i -th track, δz_i is its measurement uncertainty, and λ is the parameter for the penalty term that ensures the probability to add up to one.

The QUBO Hamiltonian was solved with a D-Wave 2000Q quantum annealer for various simplified event topologies ranging from two primary vertices and 10 tracks to five primary vertices and 15 tracks. The performance was comparable with simulated annealing for small numbers of vertices. Extending this method to larger problem sizes compatible with the LHC and HL-LHC would require an increased number of qubits and connectivity in quantum annealing hardware.

Table 3: Computational complexity of classical and quantum thrust algorithms for a single collision event with N particles.¹²³

Implementation	Time Usage	Qubit Usage
Classical ¹²⁴	$O(N^3)$	—
Classical with sort inspired by SISCONE ¹²⁵	$O(N^2 \log N)$	—
Classical with parallel sort	$O(N \log N)$	—
Quantum annealing	Gap dependent	$O(N)$
Quantum search: sequential model	$O(N^2)$	$O(\log N)$
Quantum search: parallel model	$O(N \log N)$	$O(N \log N)$

search. The former is a global reconstruction approach, which is described in Section 5.2. As the axis-finding problem, thrust T is defined as finding the optimal unit vector that maximizes $T(\hat{n})$:

$$T(\hat{n}) = \frac{\sum_{i=1}^N |\hat{n} \cdot \vec{p}_i|}{\sum_{i=1}^N |\vec{p}_i|}, \quad (22)$$

$$T = \max_{|\hat{n}|=1} T(\hat{n}), \quad (23)$$

where \hat{n} is a unit norm vector to scan and \vec{p}_i is the three momentum of the i -th particle. Table 3 summarizes the computational scaling for N particles in the final state. The most efficient classical algorithm previously known as of Ref. 123 scales as $O(N^3)$.¹²⁴ The authors first of all proposed that the classical algorithm can be improved to $O(N^2 \log N)$ with a sorting technique inspired by the SISCONE jet algorithm.¹²⁵ By introducing parallel computing models in which N parallel processors accompany N words of memory, the runtime can be further reduced to $O(N \log N)$. For quantum approaches, the authors adopted the quantum maximum finding algorithm of Dürr and Høyer,¹²⁶ which is a generalization of Grover search. For loading classical datasets into a quantum memory, they studied two computing scenarios: the sequential model and the parallel model. In the sequential model, one classical or quantum gate is executed per time step, whereas in the parallel model, all N database items are preloaded to $O(N)$ qubits at the same time. Quantum thrust algorithms generally have two abstract operations: LOOKUP and SUM.¹²³ The LOOKUP operation extracts the momentum of a particle corresponding to one index, whereas the SUM operation adds up all momenta. In the sequential (parallel) model, both the LOOKUP and SUM operations take $O(N)$ ($O(\log N)$) time. The parallel approaches with classical and quantum thrust algorithms coincidentally end up with the same $O(N \log N)$ scaling, but due to fundamentally different reasons.

Subsequent studies used the IBM Qiskit circuit simulator to actually pursue iterative quantum jet clustering.^{116,127} Ref. 116 adopted the K-means algorithm^{128,129} to inclusively reconstruct jets, iterating over N jet constituents with D -dimensional data points and outputting K jets where K is defined by the user. As the jet multiplicity is unknown ahead of time in inclusive jet reconstruction, the algorithm

Table 4: Computational complexity of classical and quantum algorithms using **K-means**, affinity propagation (AP), or sequential recombination algorithms for a single collision event with N particles, K centroids (**K-means**), T iterations (AP), and dimensions of data points D (**K-means**, AP).^{116,127}

Jet algorithms	Classical	Quantum
K-means	$O(NKD)$	$O(NK \log D)$, ¹¹⁶ $O(N \log K \log(D-1))$ ¹²⁷
AP	$O(N^2TD)$	$O(N^2T \log(D-1))$ ¹²⁷
k_t , C/A, anti- k_t	$O(N^3)$ [suboptimal] $O(N \log N)$ [FastJet] ^{132,133}	$O(N^2 \log N)$ ¹²⁷ $O(N \log N)$ ¹²⁷

iterated over a range of K and chose the jet multiplicity with the highest Silhouette Index.¹³⁰ The computing complexity scales as $O(KND)$ for the classical **K-means**, whereas it is reduced to $O(KN \log D)$ in the quantum counterpart due to the data encoding of particle momenta and jet centroids (Table 4). Jet reconstruction with quantum **K-means** resembled the k_t jet clustering¹³¹ in terms of jet constituent assignment and jet multiplicity.

In Ref. 127, the authors have introduced two novel approaches to enhance computational performance: a quantum subroutine to calculate a Minkowski-based distance between two data points and another subroutine to find the maximum from an unsorted data list. The performance of the quantum circuit was evaluated against three sets of classical benchmarks, respectively, consisting of **K-means**, affinity propagation (AP), and sequential recombination algorithms. The sequential recombination algorithms generally cluster jet constituents based on a distance measure. The Minkowski-type quantum distance was considered for the first time with the **K-means** and AP algorithms. Computing the distance would only require $O(\log(D-1))$ qubits for both the **K-means** and AP algorithms, and searching for the minimum distance with respect to the centroids would yield to $O(\log K)$ for **K-means**. Overall, the quantum **K-means** and AP algorithms achieve reduced computational complexity from the classical counterparts (Table 4). For the sequential recombination clustering, the k_t ,^{131,134,135} Cambridge/Aachen,^{136,137} and anti- k_t algorithms¹³⁸ are evaluated, for which the distance measure d_{ij} is defined as:

$$d_{ij} = \min(p_{T,i}^{2p}, p_{T,j}^{2p}) \Delta R_{ij}^2 / R^2, \quad (24)$$

$$\Delta R_{ij} = (y_i - y_j)^2 + (\phi_i - \phi_j)^2, \quad (25)$$

where i, j are the jet constituent labels; $p_{T,i}$, y_i , ϕ_i are the transverse momentum, rapidity, and azimuthal angle of the i -th jet constituent; and R is the jet-radius parameter usually taken to be between 0.4 and 1. The index parameters $p=1$ (k_t), 0 (Cambridge/Aachen), and -1 (anti- k_t) correspond to the three algorithms, respectively. The classical sequential recombination originally scaled as $O(N^3)$, but later improved to $O(N^2)$ by identifying particles' geometrical nearest neighbors, and even down to $O(N \log N)$ by further introducing the Voronoi diagrams.^{132,133} The quantum circuit brings in speed-up for the minimum search, scaling the com-

puting complexity from $O(N)$ of the classical counterpart down to $O(N \log N)$. In summary, the most efficient classical and quantum algorithms for the sequential recombination lead to the same order. Pursuing the computation on actual quantum hardware was not feasible because of the hardware noise and the lack of QuAM. Noise-free quantum circuit simulator from IBM demonstrated that the classical and quantum algorithms obtain consistent particle assignment to jets.

5.2. Global jet reconstruction

Jet reconstruction can also be formulated as a QUBO problem. The first study on global jet clustering using quantum annealing considered a thrust-based QUBO Hamiltonian:

$$O_{\text{QUBO}}(s_i) = \left(\sum_{i=1}^N |\vec{p}_i| \right)^2 T(s_i)^2, \quad (26)$$

where s_i is the binary $\{0,1\}$ that indicates which jet the i -th constituent is assigned to, N is the number of jet constituents, \vec{p}_i is the three momentum of the i -th constituent, and $T(s_i)$ is thrust defined as:

$$T(s_i) = 2 \frac{\left| \sum_{i=1}^N s_i \vec{p}_i \right|}{\sum_{i=1}^N |\vec{p}_i|}. \quad (27)$$

As described in Section 5.1, global reconstruction of thrust is defined as a partitioning problem, and thrust is defined in a slightly different formulation as the axis finding problem for the iterative reconstruction (Eq. 22). However, they are actually equivalent quantities. The performance was evaluated on the $e^+e^- \rightarrow \gamma/Z^0 \rightarrow q\bar{q}$ process with a 5000+-qubit quantum annealer D-Wave Advantage 4.1. After tuning the annealing parameters, namely, the relative chain strength, annealing time, and the number of runs per event, they observed deviations in the range of 1 to 3 % from the target value, whereas the results degraded to the deviations of 50% without the tuning. In summary, quantum annealing with tuned annealing parameters and a hybrid quantum/classical approach using the untuned annealing results as a seed for classical iterative improvement, both exhibit similar performance to exact classical approaches and heuristics.

An alternative quantum-annealing approach is to use a more generic formulation of the QUBO Hamiltonian¹³⁹ defined as in Eq. 2. In Ref. 139, the angle between the constituents is adopted as the distance:

$$Q_{ij} = -\frac{\vec{p}_i \cdot \vec{p}_j}{2(|\vec{p}_i| \cdot |\vec{p}_j|)}. \quad (28)$$

The efficiency defined below was used as the metric to evaluate the jet clustering performance:

$$\text{Efficiency} = \frac{\# \text{ of constituents clustered the same as } ee\text{-}k_t}{\# \text{ of constituents from } ee\text{-}k_t}. \quad (29)$$

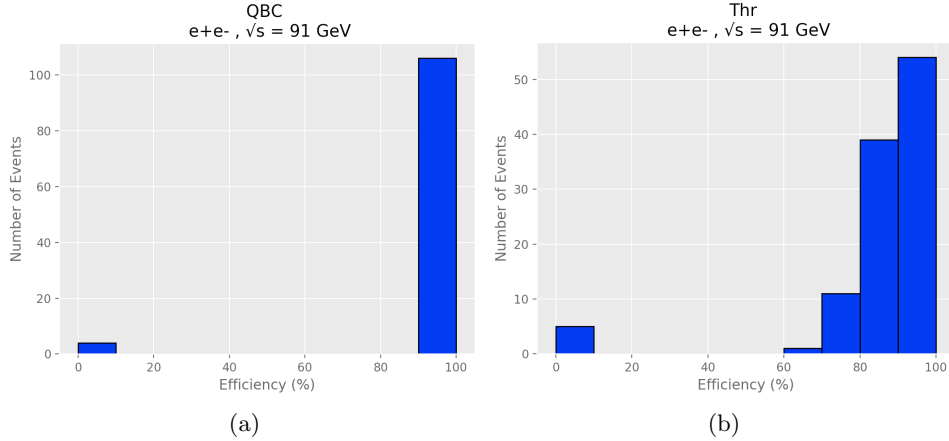


Fig. 11: Efficiency of jet clustering with (a) quantum angle-based algorithm and (b) the thrust-based algorithm. Reproduced from Ref. 139. CC BY 4.0.

As presented in Fig. 11, the angle-based dijet clustering is found to cluster jet constituents in a more consistent way than the thrust-based approach to the traditional $ee-k_t$ algorithm.¹⁴⁰

A similar study using QAOA as the Ising solver was presented in Ref. 141. It adopted the sum of the two reconstructed jets as the performance metric and was compared to the classical $ee-k_t$ and K-means algorithms. This angle-based approach with QAOA presented comparable performance to the $ee-k_t$ algorithm on simplified 6-particle and 30-particle datasets from the $e^+e^- \rightarrow ZH \rightarrow \nu\bar{\nu}s\bar{s}$ events at CEPC. Only the former dataset designed for six qubits was considered for quantum hardware computation because of the noise and limited connectivity of the BAQIS Quafu Baihua quantum processor. The classical K-means algorithm generally presented a degraded performance compared to the classical $ee-k_t$ algorithm and QAOA results.

As is evident from the binary formulation, all the above formalisms can only handle dijet clustering. In order to expand the method to multijet problems, the QUBO can be generalized to:^{57, 123, 139}

$$O_{\text{QUBO}}^{\text{multijet}}(s_i^{(n)}) = \sum_{n=1}^{n_{\text{jet}}} \sum_{i,j=1}^N Q_{ij} s_i^{(n)} s_j^{(n)} + \lambda \sum_{i=1}^N \left(1 - \sum_{n=1}^{n_{\text{jet}}} s_i^{(n)} \right)^2, \quad (30)$$

where n considers the jet multiplicity and the binary $s_i^{(n)}$ is defined for each jet. The second term serves as a constraint to ensure that each jet constituent is assigned to a jet only once. The coefficient of this penalty λ must be sufficiently large: $\lambda > N \max_{ij} Q_{ij}$.¹²³ Quantum annealing was explored for multijet reconstruction; however, employing multiple qubits for one-hot encoding is challenging and susceptible to errors.¹³⁹ Furthermore, annealing time tends to have a long duration. It remains to be seen with next-generation annealers with the increased qubit connectivity, whether we can address multijet reconstruction problems with actual

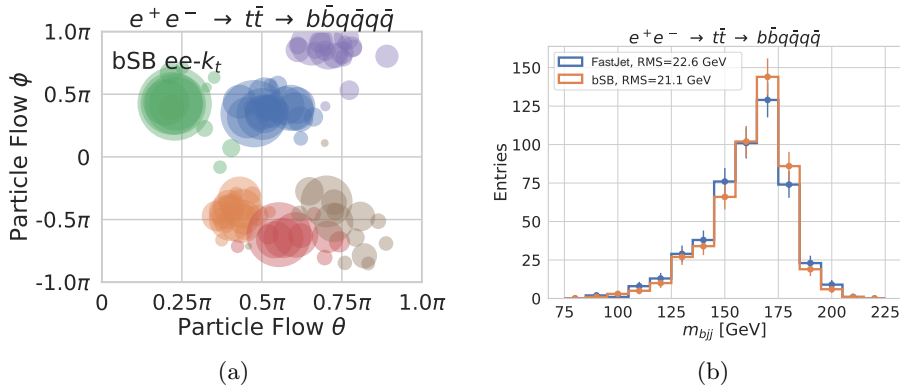
24 *Hideki Okawa*

Fig. 12: Event display for a $t\bar{t}$ event (a) and top-quark invariant mass computed from jets reconstructed by FastJet or bSB (b). Reproduced from Ref. 57. CC BY 4.0.

quantum hardware.

Meanwhile, a quantum-inspired approach using bSB succeeded in globally reconstructing multijet events with a QUBO formulation for the first time (Figure 12a).⁵⁷ The study considered $e^+e^- \rightarrow Z \rightarrow q\bar{q}$, $ZH \rightarrow q\bar{q}b\bar{b}$, and $t\bar{t} \rightarrow b\bar{b}q\bar{q}q\bar{q}$ events at CEPC, corresponding to 2, 4, and 6 jets, respectively. The distance used in the Durham or $ee-k_t$ algorithm¹⁴⁰ was adopted for the QUBO matrix:

$$Q_{ij} = 2\min(E_i^2, E_j^2)(1 - \cos\theta_{ij}), \quad (31)$$

where E_i is the energy of the i -th jet constituent, while θ_{ij} denotes the angle between the i -th and j -th jet constituents. For the all-hadronic $t\bar{t}$ events, bSB was able to find about 10 times lower minimum energy prediction compared to SA. The study also showed that the angle-based formulation is not suitable for high jet multiplicity events, and thus, the QUBO formulation has a significant impact on the multijet clustering performance. Furthermore, global reconstruction by bSB improved the jet energy resolution by 6 (7)% in the invariant mass of Higgs bosons (top quarks) from their hadronic decays. Ref. 57 also evaluated the performance of bSB against quantum annealing and QAOA for two simplified jet datasets (12 qubits) using simulators.^{142,143} Even for such small datasets, bSB outperforms the computing speed of D-Wave 2000Q by about two orders of magnitude and even more for QAOA, although it should be noted that QAOA should run faster on real quantum hardware.

5.3. Summary and Outlook

Foreseeing the HL-LHC to start operating in 2030 and other future colliders under consideration, innovations in computing are eagerly awaited. Along with the detector simulation, reconstruction, i.e., pattern recognition, is one of the most

CPU-consuming tasks at high-energy colliders. Quantum artificial intelligence could potentially bring in significant speed-up and/or allow us to perform previously unattainable computation. Investigations have been continuously pursued in the past several years.

With quantum circuit machines, various components of reconstruction could accelerate, with a caveat that quantum hardware needs to be improved in terms of error reduction, the presence of the QuAM architecture, and the number of qubits. The overhead of the classical data loading must also be carefully considered for practical applications.¹²³ Quantum annealing allows us to handle larger datasets compared to the quantum circuit machines, but the current limited connectivity has been a crucial bottleneck for jet reconstruction. Meanwhile, quantum-inspired algorithms are promising for near-term applications, demonstrating their capability to handle large datasets and excellent computing speed and ground state predictions for Ising/QUBO problems.

Nevertheless, both quantum circuit machines and quantum annealers have been continuously achieving important milestones in the past several years. Combined with High Performance Computing, quantum computing hardware may bring in paradigm shifts in HEP in the coming years. However, some components of the experimental workflow require sub-million to million-level problem sizes, which are unlikely to be reached by error-tolerant quantum hardware in the near future. Quantum-inspired techniques are valuable regardless of the near and long-term success of the quantum hardware development. The rich program of quantum computing applications in HEP is likely to progress with constructive competitions among the three quantum technologies and other emerging techniques awaiting further development and practical implementations.

Acknowledgments

HO is supported by the NSFC Basic Science Center Program for Joint Research on High Energy Frontier Particle Physics under Grant No. 12188102.

References

1. <https://quantum2025.org>.
2. W. Heisenberg, *Z. Phys.* **33**, 879 (1925).
3. M. Born, W. Heisenberg and P. Jordan, *Z. Phys.* **35**, 557 (1926).
4. L. V. P. R. de Broglie, *Annals Phys.* **2**, 22 (1925).
5. E. Schrödinger, *Annalen Phys.* **386**, 109 (1926).
6. P. A. M. Dirac, *Proc. Roy. Soc. Lond. A* **113**, 621 (1927).
7. P. Jordan, *Z. Phys.* **40**, 809 (1927).
8. G. E. Uhlenbeck and S. Goudsmit, *Naturwissenschaften* **47**, 953 (1925).
9. F. Arute *et al.*, *Nature* **574**, 505 (2019).
10. H.-S. Zhong *et al.*, *Science* **370**, 1460 (2020).
11. J. Preskill, *Quantum* **2**, 79 (2018).
12. R. Acharya *et al.*, *Nature* (2024).

13. D. Gao, D. Fan, C. Zha, J. Bei, G. Cai, J. Cai, S. Cao, F. Chen, J. Chen *et al.*, *Phys. Rev. Lett.* **134**, 090601 (2025).
14. I. Béjar Alonso, O. Brüning, P. Fessia, M. Lamont, L. Rossi, L. Tavian, M. Zerlauth (editors), *CERN Yellow Reports: Monographs* 2020.
15. ATLAS Collaboration, *CERN-LHCC-2022-005, LHCC-G-182* (2022).
16. CMS Offline Software and Computing, *CMS-NOTE-2022-008, CERN-CMS-NOTE-2022-008* (2022).
17. CEPC Study Group, *Radiat. Detect. Technol. Methods* **8**, 1 (2024).
18. CEPC Study Group (2025), [arXiv:2510.05260](https://arxiv.org/abs/2510.05260) [hep-ex].
19. W. Guan, G. Perdue, A. Pesah, M. Schuld, K. Terashi, S. Vallecorsa and J.-R. Vlimant, *Mach. Learn. Sci. Tech.* **2**, 011003 (2021).
20. H. M. Gray and K. Terashi, *Front. in Phys.* **10**, 864823 (2022).
21. A. Delgado and K. E. Hamilton, in *2022 IEEE/ACM International Conference On Computer Aided Design*, (2022).
22. A. Delgado *et al.*, in *Snowmass 2021*, (2022). [arXiv:2203.08805](https://arxiv.org/abs/2203.08805) [physics.data-an].
23. C. W. Bauer *et al.*, *PRX Quantum* **4**, 027001 (2023).
24. A. Di Meglio *et al.*, *PRX Quantum* **5**, 037001 (2024).
25. Y. Fang, C. Gao, Y.-Y. Li, J. Shu, Y. Wu, H. Xing, B. Xu, L. Xu and C. Zhou, *Sci. China Phys. Mech. Astron.* **68**, 260301 (2025).
26. Editorial, *Nature Reviews Physics* **4**, 1 (2022).
27. Y. Manin, *Mathematics as Metaphor. Selected Essays of Yuri I. Manin (American Mathematical Society, 2007), original work in Russian* (1980).
28. P. Benioff, *J. Statist. Phys.* **22**, 563 (1980).
29. R. P. Feynman, *Int. J. Theor. Phys.* **21**, 467 (1982).
30. D. David, *Proc. R. Soc. Lond. A* **400**, 97 (1985).
31. P. W. Shor, *SIAM J. Sci. Statist. Comput.* **26**, 1484 (1997).
32. Y. Nakamura, Y. A. Pashkin and J. S. Tsai, *Nature* **398**, 786 (1999).
33. T. Kadowaki and H. Nishimori, *Phys. Rev. E* **58**, 5355 (1998).
34. S. Lloyd and S. L. Braunstein, *Phys. Rev. Lett.* **82**, 1784 (1999).
35. S. Abel, M. Spannowsky and S. Williams, *Phys. Rev. A* **112**, 012614 (2025).
36. B. Maier, M. Spannowsky and S. Williams (10 2025), [arXiv:2510.13994](https://arxiv.org/abs/2510.13994) [quant-ph].
37. https://docs.dwavequantum.com/en/latest/quantum_research/quantum_annealing_intro.html.
38. A. Barenco, C. H. Bennett, R. Cleve, D. P. DiVincenzo, N. Margolus, P. Shor, T. Sleator, J. A. Smolin and H. Weinfurter, *Phys. Rev. A* **52**, 3457 (1995).
39. M. A. Nielsen and I. L. Chuang, *Quantum Computation and Quantum Information: 10th Anniversary Edition* (Cambridge University Press, 2010).
40. Q.-G. Zeng, X.-P. Cui, B. Liu, Y. Wang, P. Mosharev and M.-H. Yung, *Commun. Phys.* **7**, 249 (2024).
41. S. Kirkpatrick, C. D. Gelatt and M. P. Vecchi, *Science* **220**, 671 (1983).
42. E. S. Tiunov, A. E. Ulanov and A. I. Lvovsky, *Opt. Express* **27**, 10288 (2019).
43. H. Goto, K. Tatsumura and A. R. Dixon, *Science Advances* **5**, eaav2372 (2019).
44. H. Goto, K. Endo, M. Suzuki, Y. Sakai, T. Kanao, Y. Hamakawa, R. Hidaka, M. Yamasaki and K. Tatsumura, *Science Advances* **7**, eabe7953 (2021).
45. T. Kanao and H. Goto, *Commun. Phys.* **5**, 153 (2022).
46. L. Borella, A. Coppi, J. Pazzini, A. Stanco, M. Trenti, A. Triossi and M. Zanetti (2024), [arXiv:2409.16075](https://arxiv.org/abs/2409.16075) [hep-ex].
47. S. Abel, M. Spannowsky and S. Williams (2025), [arXiv:2506.17388](https://arxiv.org/abs/2506.17388) [quant-ph].

48. J. Y. Araz and M. Spannowsky, *JHEP* **08**, 112 (2021).
49. A. Lucas, *Front. in Phys.* **2**, 5 (2014).
50. A. Peruzzo, J. McClean, P. Shadbolt, M.-H. Yung, X.-Q. Zhou, P. J. Love, A. Aspuru-Guzik and J. L. O'Brien, *Nature Communications* **5** (2014).
51. E. Farhi, J. Goldstone and S. Gutmann (2014), [arXiv:1411.4028 \[quant-ph\]](#).
52. E. Farhi, J. Goldstone and S. Gutmann (2014), [arXiv:1412.6062 \[quant-ph\]](#).
53. X. Wang, Y. Chai, X. Feng, Y. Guo, K. Jansen and C. Tüysüz, *Phys. Rev. A* **111**, 032612 (2025).
54. Y. Chai and A. Di Tucci (2025), [arXiv:2505.22924 \[quant-ph\]](#).
55. M. Saito, P. Calafiura, H. Gray, W. Lavrijsen, L. Linder, Y. Okumura, R. Sawada, A. Smith, J. Tanaka and K. Terashi, *EPJ Web Conf.* **245**, 10006 (2020).
56. H. Okawa, Q.-G. Zeng, X.-Z. Tao and M.-H. Yung, *Comput. Softw. Big Sci.* **8**, 16 (2024).
57. H. Okawa, X.-Z. Tao, Q.-G. Zeng and M.-H. Yung, *Phys. Lett. B* **864**, 139393 (2025).
58. N. Metropolis, A. W. Rosenbluth, M. N. Rosenbluth, A. H. Teller and E. Teller, *Journal of Chemical Physics* **21**, 1087 (1953).
59. B. Leimkuhler and S. Reich, *Simulating Hamiltonian Dynamics* (Cambridge University Press, 2005).
60. Ai, X., Allaire, C., Calace, N. et al., *Comput Softw Big Sci* **6**, 8 (2022).
61. Exa.TrkX Collaboration, X. Ju et al., *Eur. Phys. J. C* **81**, 876 (2021).
62. X. Jia, X. Qin, T. Li, X. Huang, X. Zhang, N. Yin, Y. Zhang and Y. Yuan, *EPJ Web Conf.* **295**, 09006 (2024).
63. L. Reuter et al., *Comput. Softw. Big Sci.* **9**, 6 (2025).
64. S. Caron, N. Dobрева, A. F. Sánchez, J. D. Martín-Guerrero, U. Odyurt, R. R. Ruiz de Austri Bazan, Z. Wolffs and Y. Zhao, *Eur. Phys. J. C* **85**, 460 (2025).
65. S. Caron, N. Dobрева, M. Kimpel, U. Odyurt, S. Pshenov, R. Ruiz de Austri Bazan, E. Shalugin, Z. Wolffs and Y. Zhao (2025), [arXiv:2509.26411 \[hep-ex\]](#).
66. S. V. Stroud, P. Duckett, M. Hart, N. Pond, S. Rettie, G. Facini and T. Scanlon, *Phys. Rev. X* (2025).
67. A. Nikolskaia, P. Goncharov, G. Ososkov et al., *Phys. Part. Nuclei* **56**, 1555–1559 (2025).
68. S. Amrouche et al., *The NeurIPS '18 Competition: From Machine Learning to Intelligent Conversations* (2019), [arXiv:1904.06778 \[hep-ex\]](#).
69. S. Amrouche et al., *Comput. Softw. Big Sci.* **7**, 1 (2023).
70. B. H. Denby, *Comput. Phys. Commun.* **49**, 429 (1988).
71. C. Peterson, *Nucl. Instrum. Meth. A* **279**, 537 (1989).
72. G. Stimpfl-Abele and L. Garrido, *Computer Physics Communications* **64**, 46 (1991).
73. S. Baginian, A. Glazov, I. Kisel, E. Konotopskaya, V. Neskoromnyi and G. Ososkov, *Comput. Phys. Commun.* **79**, 165 (1994).
74. A. Pulvirenti, A. Badala, R. Barbera, G. Lo Re, A. Palmeri, G. S. Pappalardo and F. Riggi, *Nucl. Instrum. Meth. A* **533**, 543 (2004).
75. G. Passaleva, in *2008 IEEE Nuclear Science Symposium and Medical Imaging Conference and 16th International Workshop on Room-Temperature Semiconductor X-Ray and Gamma-Ray Detectors*, (2008). pp. 867–872.
76. A. Zlokapa, A. Anand, J.-R. Vlimant, J. M. Duarte, J. Job, D. Lidar and M. Spiropulu, *Quantum Machine Intelligence* **3**, 27 (2021).
77. F. Bapst, W. Bhimji, P. Calafiura, H. Gray, W. Lavrijsen and L. Linder, *Comput. Softw. Big Sci.* **4**, 1 (2020).
78. T. Sjostrand, S. Mrenna and P. Z. Skands, *Comput. Phys. Commun.* **178**, 852 (2008).
79. D. Nicotra, M. Lucio Martinez, J. A. de Vries, M. Merk, K. Driessens, R. L. Westra,

- D. Dibenedetto and D. H. Cámpora Pérez, *JINST* **18**, P11028 (2023).
80. D. H. Cámpora Pérez, N. Neufeld and A. Riscos Núñez, *Journal of Computational Science* **54**, 101422 (2021).
 81. A. W. Harrow, A. Hassidim and S. Lloyd, *Phys. Rev. Lett.* **103**, 150502 (2009).
 82. D. Nicotra, dnicotra/TrackHHL: A quantum algorithm for track reconstruction using HHL (July 2023).
 83. L. Funcke, T. Hartung, B. Heinemann, K. Jansen, A. Kropf, S. Kühn, F. Meloni, D. Spataro, C. Tüysüz and Y. C. Yap, *J. Phys. Conf. Ser.* **2438**, 012127 (2023).
 84. A. Crippa *et al.*, *Comput. Softw. Big Sci.* **7**, 14 (2023).
 85. T. Schwägerl, C. Issever, K. Jansen, T. J. Khoo, S. Kühn, C. Tüysüz and H. Weber (2023), [arXiv:2303.13249](https://arxiv.org/abs/2303.13249) [quant-ph].
 86. H. Abramowicz *et al.*, *Eur. Phys. J. ST* **230**, 2445 (2021).
 87. H. Okawa, *Springer Communications in Computer and Information Science* **2036**, 272 (2024), [arXiv:2310.10255](https://arxiv.org/abs/2310.10255) [quant-ph].
 88. Y. Atobe, M. Tawada and N. Togawa, *IEEE Trans. Comp.* **71**, 2606 (2022).
 89. G. Quiroz, L. Ice, A. Delgado and T. S. Humble, *Nucl. Instrum. Meth. A* **1010**, 165557 (2021).
 90. H. Seddiqi and T. S. Humble, *Front. Phys.* **2**, 79 (12 2014).
 91. S. Santra, O. Shehab and R. Balu, *Phys. Rev. A* **96**, 062330 (2017).
 92. J. Schrock, A. McCaskey, K. Hamilton, N. Imam and T. Humble, *Entropy* **19** (2017), Publisher Copyright: © 2017 by the authors. Licensee MDPI, Basel, Switzerland.
 93. C. Tüysüz, C. Rieger, K. Novotny, B. Demirköz, D. Dobos, K. Potamianos, S. Vallecorsa, J.-R. Vlimant and R. Forster, *Quantum Machine Intelligence* **3**, 29 (2021).
 94. C. Rieger, C. Tüysüz, K. Novotny, S. Vallecorsa, B. Demirköz, K. Potamianos, D. Dobos and J.-R. Vlimant, *EPJ Web Conf.* **251**, 03065 (2021).
 95. ATLAS Collaboration, W. Y. Chan, D. Akiyama, K. Arakawa, S. Ganguly, T. Kaji, R. Sawada, J. Tanaka, K. Terashi and K. Yorita, *Application of quantum computing techniques in particle tracking at LHC*, tech. rep., CERN (Geneva, 2023).
 96. P. Duckett, G. Facini, M. Jastrzebski, S. Malik, T. Scanlon and S. Rettie, *Phys. Rev. D* **109**, 052002 (2024).
 97. D. Ventura and T. Martinez, *Info. Sci.* **124**, 273 (1998).
 98. A. Ezhov, A. Nifanova and D. Ventura, *Information Sciences* **128**, 271 (2000).
 99. C. A. Trugenberger, *Phys. Rev. Lett.* **87**, 067901 (2001).
 100. I. Shapoval and P. Calafiura, *EPJ Web Conf.* **214**, 01012 (2019).
 101. D. Magano *et al.*, *Phys. Rev. D* **105**, 076012 (2022).
 102. CMS Collaboration, S. Chatrchyan *et al.*, *JINST* **9**, P10009 (2014).
 103. L. K. Grover, *Phys. Rev. Lett.* **79**, 325 (1997).
 104. M. Boyer, G. Brassard, P. Høyer and A. Tapp, *Fortschritte der Physik* **46**, 493 (1998).
 105. C. Durr and P. Hoyer (1999), [arXiv:quant-ph/9607014](https://arxiv.org/abs/quant-ph/9607014) [quant-ph].
 106. C. Brown, M. Spannowsky, A. Tapper, S. Williams and I. Xiotidis, *Front. Artif. Intell.* **7**, 1339785 (2024).
 107. A. Bardi *et al.*, *Nucl. Instrum. Meth. A* **409**, 658 (1998).
 108. R. Nicolaidou, L. Chevalier, S. Hassani, J. F. Laporte, E. Le Menedeu and A. Ouraou, *J. Phys. Conf. Ser.* **219**, 032052 (2010).
 109. CMS Collaboration, K. Bunkowski, *Nucl. Instrum. Meth. A* **936**, 368 (2019).
 110. ATLAS Collaboration, G. Aad *et al.*, *JINST* **16**, P07006 (2021).
 111. G. Brassard, P. Hoyer, M. Mosca and A. Tapp, *Quantum Computation and Information*, 53–74 (2002).
 112. V. Giovannetti, S. Lloyd and L. Maccone, *Phys. Rev. Lett.* **100**, 160501 (2008).
 113. V. V. Shende, S. S. Bullock and I. L. Markov, *IEEE Trans. Comput. Aided Design*

- Integr. Circuits Syst.* **25**, 1000 (2006).
114. S. Gao, F. Hayes, S. Croke, C. Messenger and J. Veitch, *Phys. Rev. Res.* **4**, 023006 (2022).
 115. S. Das, A. J. Wildridge, S. B. Vaidya and A. Jung (2019), [arXiv:1903.08879 \[hep-ex\]](#).
 116. D. Pires, P. Bargassa, J. Seixas and Y. Omar (2021), [arXiv:2101.05618 \[physics.data-an\]](#).
 117. G. F. Sterman and S. Weinberg, *Phys. Rev. Lett.* **39**, 1436 (1977).
 118. S. Moretti, L. Lonnblad and T. Sjostrand, *JHEP* **08**, 001 (1998).
 119. G. C. Blazey, J. R. Dittmann, S. D. Ellis, V. D. Elvira, K. Frame, S. Grinstein, R. Hirosky, R. Piegaiia, H. Schellman, R. Snihur, V. Sorin and D. Zeppenfeld (2000), [arXiv:hep-ex/0005012 \[hep-ex\]](#).
 120. S. D. Ellis, J. Huston, K. Hatakeyama, P. Loch and M. Tonnesmann, *Prog. Part. Nucl. Phys.* **60**, 484 (2008).
 121. G. P. Salam, *Eur. Phys. J. C* **67**, 637 (2010).
 122. A. Ali and G. Kramer, *Eur. Phys. J. H* **36**, 245 (2011).
 123. A. Y. Wei, P. Naik, A. W. Harrow and J. Thaler, *Phys. Rev. D* **101**, 094015 (2020).
 124. H. Yamamoto, *J. Comput. Phys.* **52**, 597 (1983).
 125. G. P. Salam and G. Soyez, *JHEP* **05**, 086 (2007).
 126. C. Durr and P. Hoyer (1996), [arXiv:quant-ph/9607014](#).
 127. J. J. Martínez de Lejarza, L. Cieri and G. Rodrigo, *Phys. Rev. D* **106**, 036021 (2022).
 128. J. MacQueen, in *Proc. Fifth Berkeley Symposium on Math. Stat. and Prob.*, (1967).
 129. G. H. Ball and D. J. Hall, *Behav. Sci.* **12**, 153 (2010).
 130. P. J. Rousseeuw, *Journal of Computational and Applied Mathematics* **20**, 53 (1987).
 131. S. Catani, Y. L. Dokshitzer, M. H. Seymour and B. R. Webber, *Nucl. Phys. B* **406**, 187 (1993).
 132. M. Cacciari and G. P. Salam, *Phys. Lett. B* **641**, 57 (2006).
 133. M. Cacciari, G. P. Salam and G. Soyez, *Eur. Phys. J. C* **72**, 1896 (2012).
 134. S. D. Ellis and D. E. Soper, *Phys. Rev. D* **48**, 3160 (1993).
 135. M. Dasgupta and G. P. Salam, *JHEP* **03**, 017 (2002).
 136. Y. L. Dokshitzer, G. D. Leder, S. Moretti and B. R. Webber, *JHEP* **08**, 001 (1997).
 137. M. Wobisch and T. Wengler, 270 (1998), [arXiv:hep-ph/9907280](#).
 138. M. Cacciari, G. P. Salam and G. Soyez, *JHEP* **04**, 063 (2008).
 139. D. Pires, Y. Omar and J. Seixas, *Physics Letters B* **843**, 138000 (2023).
 140. S. Catani, Y. Dokshitzer, M. Olsson, G. Turnock and B. Webber, *Physics Letters B* **269**, 432 (1991).
 141. Y. Zhu, W. Zhuang, C. Qian, Y. Ma, D. E. Liu, M. Ruan and C. Zhou, *Science Bulletin* **70**, 460 (2025).
 142. Z. Morrell, M. Vuffray, S. Misra and C. Coffrin (2024), [arXiv:2404.14501 \[quant-ph\]](#).
 143. X. Xu et al. (2024), [arXiv:2406.17248 \[quant-ph\]](#).